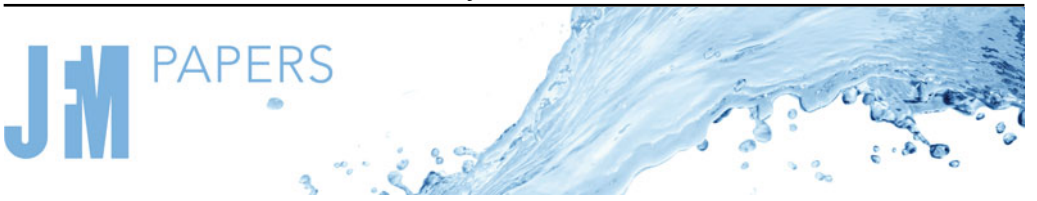
J. Fluid Mech. (2026), *vol.* 1026, A36, doi:10.1017/jfm.2025.11023



Enthalpy transformation for wall-bounded supercritical flows with heat transfer

Teng Wan[1,2], **Pei-Xue Jiang**[1], **Pinghui Zhao**[3] **and Xingjian Wang**[1]

[1]Department of Energy and Power Engineering, Tsinghua University, Beijing 100084, PR China

[2]College of Energy and Power Engineering, Nanjing University of Aeronautics and Astronautics, Nanjing 210016, PR China

[3]Institute of Plasma Physics Chinese Academy of Sciences, Hefei 230031, PR China

Corresponding author: Xingjian Wang, xingjianwang@tsinghua.edu.cn

(Received 2 June 2025; revised 15 October 2025; accepted 30 November 2025)

Fluids at supercritical pressure (SCP) exhibit significant real-fluid effects across the pseudo-critical point, which challenges the validity of the existing wall-scaling laws developed under atmospheric pressure condition. This study revisits prior efforts on the temperature-based transformation for the collapse of mean scalar profiles, emphasising the difficulties in accurately describing universal characteristics of thermal boundary layers at SCP. To address this, a novel thermal scaling law using enthalpy transformation is proposed by incorporating the chain rule and heat flux balance. This transformation effectively accounts for variations in the near-wall thermophysical properties associated with the scalar profile while excluding the gradient of isobaric specific heat capacity-related terms. The proposed scaling law demonstrates substantially improved alignment of transformed mean scalar profiles in SCP channel flows at different wall-temperature differences and Reynolds numbers. Additionally, the enthalpy transformation shows superior performance compared with the existing enthalpy–velocity relations, particularly near the heated-wall region where the fluid thermodynamic states undergo the pseudo-boiling process. The present work could facilitate the development of universal wall model in supercritical flows, enabling rapid and reliable heat transfer predictions in practical applications.

Key words: turbulent flows, turbulence simulation, turbulence modelling

1. Introduction

The law of the wall remains a cornerstone of turbulence theory in wall-bounded flows by offering one of the few analytical descriptions of the mean-field behaviour (Bradshaw & Huang 1995). Originally developed for incompressible, constant-property flows (Prandtl

© The Author(s), 2026. Published by Cambridge University Press.

https://doi.org/10.1017/jfm.2025.11023 Published online by Cambridge University Press

1925; Von Karman 1939; Bradshaw & Huang 1995; Buschmann & Gad-el-Hak 2006), the law of the wall has served as the basis for configuring wall functions in turbulence modelling by providing a simple yet powerful scaling for mean-velocity profiles. The wall-scaling law for mean velocity (V-law) was later extended to compressible regimes (Van Driest 1951; Huang, Coleman & Bradshaw 1995; Zhang *et al.* 2012; Trettel & Larsson 2016; Griffin, Fu & Moin 2021; Hasan *et al.* 2023; Zhu *et al.* 2024), where the mean property variations induced by Mach number are non-negligible. While considerable efforts have been devoted to the V-law, the studies on the thermal boundary layer (T-law) have been relatively underdeveloped, particularly at supercritical pressure (SCP), a typical condition encountered in many practical applications, such as liquid rocket engines (Yang 2000; Wang *et al.* 2018), regenerative cooling (Xie *et al.* 2022) and thermal power cycles (White *et al.* 2021). Supercritical pressure fluids exhibit steep gradients and strong nonlinearities in thermophysical properties such as specific heat capacity, thermal conductivity, dynamic viscosity and density, particularly near the pseudo-boiling regime (Jiang *et al.* 2008). These variations impact both the mean flow and its stability characteristics, giving rise to inviscid instabilities and increased sensitivity to perturbations. In such regimes, the mean velocity and temperature profiles may develop inflectional features across the Widom line (Ren *et al.* 2025), further complicating the applicability of classical scaling arguments. The existing temperature-based thermal transformations for the T-law (Kader 1981; Patel, Boersma & Pecnik 2017; Guo, Yang & Ihme 2018) often fail to provide consistent scaling under these conditions. This further motivates us to establish a universal thermal transformation at SCP, which would be of theoretical interest and practical significance for reduced-order turbulence wall modelling.

1.1. *The law of the wall – velocity scaling*

Advancements in the wall-scaling law in compressible boundary layers mainly stem from the foundational work of Van Driest (VD) (1951), who proposed the velocity transformation (namely, VD transformation or VDT) grounded in Morkovin's scaling and Prandtl's incompressible mixing length theory. However, the VDT does not perform well for diabatic boundary layers and channel flows. To address this issue, Zhang *et al.* (2012) introduced a viscosity-weighted transformation of the mean-velocity profile based on a boundary-layer thickness length scale using Reynolds stress structure parameters to fulfil the Mach-number-invariant condition. The performance improvement was found to be still limited under diabatic conditions (Griffin *et al.* 2021; Hasan *et al.* 2023). Huang *et al.* (1995) developed a semi-local scaling method to enhance the mapping of wall-normal turbulence statistics in the logarithmic region. Pecnik & Patel (2017) provided theoretical support for the semi-local scaling and identified the quasi-similarity between variable-property and constant-property flows. Ma, Yang & Ihme (2018) examined this approach under transcritical conditions and reported reduced effectiveness near the heated wall, where density fluctuation is stronger than at the cooled wall. Trettel & Larsson (TL) (2016) incorporated the stress balance assumption and developed a new transformation (namely, TL transformation) to overcome the VDT's insufficiency for non-adiabatic wall-bounded flows. The TL-transformed mean-velocity profiles collapse consistently at various Reynolds numbers, Mach numbers and wall heat transfer rates in supersonic channel flows. Wan *et al.* (2020) and Bai, Griffin & Fu (2022) demonstrated that the TL transformation works well for the inner region of the boundary layer in supercritical channel flows. More recent efforts by Griffin *et al.* (2021) integrated the frameworks of Zhang *et al.* (2012) and Trettel & Larsson (2016), and derived a new transformation

https://doi.org/10.1017/jfm.2025.11023 Published online by Cambridge University Press

based on the universality of the production-to-consumption ratio and a stress-based mixing function, yet their approach struggles with non-air-like viscosity laws and SCP conditions. Hasan *et al.* (2023) accounted for intrinsic compressibility effects and extended the capabilities of the TL transformation to a broader range of flow scenarios, covering wall-bounded flows of both ideal gases and SCP fluids. However, Zhu *et al.* (2024) revealed that the efficacy of both the Griffin's and Hasan's transformations is diminished in low Reynolds number channel and pipe flows. A more complex transformation that incorporates intrinsic compressibility effects and the multi-layer structure of mixing lengths was developed, whereas its performance in SCP regimes remains unconfirmed.

1.2. *The law of the wall – temperature-/enthalpy–velocity relations*

Regarding the studies of thermal scaling, one major line of the research is on the similarity between velocity and temperature fields to establish a temperature–velocity (T–V) relation. Unlike coordinate-based wall-scaling laws, this approach is generally regarded as a weaker form of scaling (Chen *et al.* 2022). An early T–V relation was established by Busemann (1931), who showed that, for compressible laminar boundary layers with a molecular Prandtl number (Pr) of unity, velocity and temperature follow a quadratic relation. Walz (1969) later modified this relation to account for the deviation of Pr from unity through the introduction of a recovery factor, $r = Pr^{1/3}$

$$\tilde{T}_{Walz} = \tilde{T}_w + \left(\tilde{T}_r - \tilde{T}_w\right)\frac{\tilde{u}}{\tilde{u}_e} + \left(\tilde{T}_e - \tilde{T}_r\right)\left(\frac{\tilde{u}}{\tilde{u}_e}\right)^2, \tag{1.1}$$

where T and u denote temperature and velocity, with subscripts 'w' and 'e' referring to wall and boundary-layer-edge values, respectively. The recovery temperature is defined as $\tilde{T}_r = \tilde{T}_e + r\tilde{u}_e^2/(2c_p)$, and c_p is specific heat capacity at constant pressure. The tilde ($\tilde{}$) denotes a Favre-averaged quantity. While (1.1) showed good performance for adiabatic compressible turbulent boundary layers, it deviates significantly from direct numerical simulation (DNS) data under strong cold-wall conditions (Duan & Martin 2011; Zhang *et al.* 2014). To address these limitations, Zhang *et al.* (2014) introduced a generalised recovery factor, r_g to revise $\tilde{T}_{Walz}$ by incorporating cold-wall and diabatic effects. A local generalised recovery temperature $\tilde{T}_{r_g}$ was defined to replace $\tilde{T}_r$

$$\tilde{T}_{Zhang} = \tilde{T}_w + \left(\tilde{T}_{r_g} - \tilde{T}_w\right)\frac{\tilde{u}}{\tilde{u}_e} + \left(\tilde{T}_e - \tilde{T}_{r_g}\right)\left(\frac{\tilde{u}}{\tilde{u}_e}\right)^2, \tag{1.2}$$

where $\tilde{T}_{r_g} = \tilde{T}_e + r_g\tilde{u}_e^2/(2c_p)$ and $r_g = (\tilde{T}_w - \tilde{T}_e)/(\tilde{u}_e^2/(2c_p)) + (2c_p/\tilde{u}_e)(\partial\tilde{T}/\partial\tilde{u})_w$. Equation (1.2) was shown to perform well in hypersonic turbulent boundary layers of calorically perfect gases, where c_p is constant (Zhang, Duan & Choudhari 2018; Mo *et al.* 2023). However, its applicability to wall-bounded SCP flows remains to be confirmed, as real-fluid effects caused by abrupt property variations render the perfect-gas assumption invalid. In particular, c_p varies dramatically and nonlinearly across the pseudo-boiling line, complicating the relation between enthalpy and temperature in the energy transport.

To mitigate the explicit dependence of T–V relations on thermal and chemical models, Duan & Martin (2011) introduced the concept of recovery enthalpy, $\tilde{h}_r = \tilde{h} + r(\tilde{u}^2/2)$, and established a semi-empirical enthalpy–velocity (H–V) relation

$$\tilde{h} = \tilde{h}_w + \left(\tilde{h}_r - \tilde{h}_w\right) f\left(\frac{\tilde{u}}{\tilde{u}_e}\right) - \frac{r\tilde{u}^2}{2}, \tag{1.3}$$

https://doi.org/10.1017/jfm.2025.11023 Published online by Cambridge University Press

where the recovery factor r is assumed to be 0.9, and the empirical function $f(\tilde{u}/\tilde{u}_e)$ is given by fitting the DNS data of hypersonic reacting turbulent boundary layers

$$f\left(\frac{\tilde{u}}{\tilde{u}_e}\right) = 0.8259\frac{\tilde{u}}{\tilde{u}_e} + 0.1741\left(\frac{\tilde{u}}{\tilde{u}_e}\right)^2. \tag{1.4}$$

For calorically perfect gases, (1.3) reduces to the classical Walz's relation (1.1) with $\tilde{u}/\tilde{u}_e$ replaced by $f(\tilde{u}/\tilde{u}_e)$. However, its empirical nature, including a constant recovery factor and data-fitted function $f(\tilde{u}/\tilde{u}_e)$, may jeopardise its reliability for SCP conditions, where property variations are far more drastic. Inspired by Duan & Martin (2011) and Zhang *et al.* (2014), Li *et al.* (2025) have recently developed a new H-V relation without empirical function $f(\tilde{u}/\tilde{u}_e)$ but introduced the generalised recovery enthalpy $\tilde{h}_{r_g^*}$

$$\tilde{h} = \tilde{h}_w + \left(\tilde{h}_{r_g^*} - \tilde{h}_w\right)\frac{\tilde{u}}{\tilde{u}_e} + \left(\tilde{h}_e - \tilde{h}_{r_g^*}\right)\left(\frac{\tilde{u}}{\tilde{u}_e}\right)^2. \tag{1.5}$$

The generalised recovery enthalpy $\tilde{h}_{r_g^*}$ is determined as

$$\tilde{h}_{r_g^*} = \tilde{h}_e + r_g^*\tilde{u}_e^2/2, \tag{1.6}$$

and the recovery factor r_g^* defined as

$$r_g^* = \left(\tilde{h}_w - \tilde{h}_e\right)/\left(\tilde{u}_e^2/2\right) + 2Pr_w\,\bar{q}_w/(\tilde{u}_e\bar{\tau}_w). \tag{1.7}$$

Numerical studies (Li *et al.* 2025) of hypersonic reacting turbulent boundary layers at atmospheric pressure confirmed the improved accuracy of this relation.

Despite these advances, existing T–V and H–V relations were developed primarily for compressible flows under near-atmospheric conditions. Their extension to SCP wall-bounded flows remains uncertain due to the strong influence of real-fluid effects. Moreover, recent studies (Chen *et al.* 2022; Cheng & Fu 2024) argue that these relations are not closed by themselves, and limited by both the empirical recovery factor and outer boundary conditions, which prevents their application to complex flow configurations. In § 4.1, an assessment of H–V relations for SCP fluid flows will be conducted.

1.3. *The law of the wall – thermal transformation*

Another category for thermal scaling is to develop transformation-based thermal wall models that map the mean scalar profile of compressible flows into its 'incompressible' equivalent form. Recently, Chen, Gan & Fu (2025) have demonstrated that the temperature-transformation wall model for compressible laminar and turbulent flows at atmospheric pressure serves as a good alternative to the T–V wall model and successfully excludes the dependence on boundary-layer-edge quantities. However, compared with velocity transformation, thermal transformation faces additional complexity due to dependencies on heat flux, specific heat capacity and thermal conductivity (Bradshaw & Huang 1995). Furthermore, most studies on thermal boundary layers have primarily focused on flows under the ideal-gas assumption and cannot be directly extended to SCP fluid flows, where real-fluid effects play a critical role. Early efforts, such as Kader's temperature transformation (Kader 1981) based on the Reynolds analogy, were made for low-speed incompressible flows and assumed constant thermophysical properties

$$\overline{\theta}^+ = \frac{\overline{\theta}}{\overline{\theta}_\tau} = \begin{cases} Pr_w y^+ & \text{sublayer region,} \\ \frac{1}{\kappa}\ln(y^+) + \beta(Pr_w) & \text{logarithmic region.} \end{cases} \tag{1.8}$$

https://doi.org/10.1017/jfm.2025.11023 Published online by Cambridge University Press

Here, overbar $\overline{(\cdot)}$ denotes the Reynolds-averaged physical quantity, and the mean temperature difference is defined as $\overline{\theta} = \overline{T} - \overline{T}_w$; κ is a constant of 0.47; $\beta(Pr_w)$ is another constant determined by the wall Prandtl number Pr_w and is given by $\beta(Pr_w) = (3.85Pr_w^{1/3} - 1.3)^2 + 2.12\ln(Pr_w)$. The friction temperature is defined as $\overline{\theta}_\tau = \overline{q}_w/(\overline{\rho}_w\,\overline{c_p}_w\,\overline{u}_\tau)$, where q, ρ and u_τ are the heat flux, density and wall friction velocity, respectively. Hereinafter, the wall-normal coordinates y, y^+ and y^* denote the physical coordinate, the coordinate scaled by the wall viscous length δ_v^+ (Pope 2001) and the coordinate scaled by the semi-local viscous length δ_v^* (Huang *et al.* 1995), respectively. Specifically,

$$y^+ = \frac{y}{\delta_v^+},\ y^* = \frac{y}{\delta_v^*},\ \delta_v^+ = \frac{\overline{\mu}_w}{\overline{\rho}_w\,\overline{u}_\tau},\ \delta_v^* = \frac{\overline{\mu}(y)}{\overline{\rho}(y)\,\overline{u}_\tau^*},\ \overline{u}_\tau = \sqrt{\frac{\overline{\tau}_w}{\overline{\rho}_w}},\ \overline{u}_\tau^* = \sqrt{\frac{\overline{\tau}_w}{\overline{\rho}(y)}}, \tag{1.9}$$

with μ and τ_w being dynamic viscosity and viscous shear stress.

Note that (1.8), which does not account for property variations, is generally inapplicable to compressible or other variable-property flows. Lee *et al.* (2014) modified Kader's formulation by incorporating semi-local Prandtl number Pr^* instead of the wall-based Pr_w. Nonetheless, their method was pointed out to be inadequate because of neglecting the impact of property variations on the log-law slope. Patel *et al.* (2017) prescribed the relations for density ρ, viscosity μ and thermal conductivity λ as functions of temperature and derived a temperature scaling using the semi-local coordinate. This allows the influence of property variations to be parameterised by the semi-local Reynolds number Re_τ^* and Prandtl number Pr^*. The transformed mean scalar is expressed as

$$\overline{\theta}^* = \int_0^{\overline{\theta}_{VD}^+} \left[1 + \frac{y}{Re_\tau^*}\frac{\mathrm{d}Re_\tau^*}{\mathrm{d}y}\right] \mathrm{d}\overline{\theta}_{VD}^+ = \int_0^{y^*} \frac{1}{\alpha_t/\overline{\mu} + 1/Pr^*}\mathrm{d}y^*, \tag{1.10}$$

where

$$\mathrm{d}\overline{\theta}_{VD}^+ = \sqrt{\frac{\overline{\rho}(y)}{\overline{\rho}_w}}\, d\left(\frac{\overline{\theta}}{\overline{\theta}_\tau}\right),\ Re_\tau^* = Re_\tau\sqrt{\frac{\overline{\rho}(y)}{\overline{\rho}_w}}\,\frac{\overline{\mu}_w}{\overline{\mu}(y)},\ Pr^* = Pr_w\,\frac{\overline{\mu}(y)/\overline{\mu}_w}{\overline{\lambda}(y)/\overline{\lambda}_w}. \tag{1.11}$$

Here, $\bar{\theta}_{VD}^+$ denotes the VD-type temperature, and $\alpha_t = -\bar{\rho}\,\widetilde{v''\theta''}/(\mathrm{d}\bar{\theta}/\mathrm{d}y)$ represents the turbulent heat conductivity. The transformed scalar $\bar{\theta}^*$ is independent of Re_τ^* while exhibiting a Pr^*-dependent shift. Chen *et al.* (2022) extended these transformations to channel and boundary-layer flows with varying wall conditions. Huang *et al.* (2023) simplified the expression by leveraging analogies with incompressible transport equations. More recently, Cheng & Fu (2024) introduced a Mach-independent thermal scaling law at a given constant Prandtl number. In SCP wall-bounded flows, however, c_p and λ feature sharp temperature-dependent variations, leading to varying local Prandtl number in energy transport, which must be taken into account.

Establishing a reliable thermal scaling law at SCP is more challenging due to the strongly nonlinear variations of thermophysical properties near the pseudo-critical temperature T_{pc}, which is defined as the temperature at which c_p peaks (Jiang *et al.* 2008; Yoo 2013). The interplay of these abnormal property variations and the near-wall turbulent dynamics poses challenges to the validity of existing thermal transformation rules developed at atmospheric pressure. Guo, Yang & Ihme (2022) adopted Patel's transformation at SCP and reported poor collapse of transformed mean scalar profiles, likely attributed to its insufficient treatment of near-wall property variations. To address this issue, Wan *et al.* (2020) modified Patel's transformation by incorporating variable $\bar{c}_p$

https://doi.org/10.1017/jfm.2025.11023 Published online by Cambridge University Press

into the semi-local Prandtl number ($Pr^* = Pr_w\bar{\mu}(y)\bar{c}_p(y)\bar{\lambda}_w/(\bar{\mu}_w\overline{c_p}_w\bar{\lambda}(y))$) and the VD-type temperature gradient ($\mathrm{d}\bar{\theta}^+_{VD}/\mathrm{d}y = \sqrt{\bar{\rho}(y)/\bar{\rho}_w}\bar{c}_p(y)/\overline{c_p}_w d(\bar{\theta}/\bar{\theta}_\tau)/\mathrm{d}y$). While the modified transformation improved the collapse of the slopes in logarithmic region at small wall-temperature differences, it still performs unsatisfactorily in capturing the overall transformed temperature profiles. Toki, Teramoto & Okamoto (2020) proposed a VD-based temperature transformation that incorporates the variation of $\bar{c}_p$ at SCP and the mixing length hypothesis for energy transport with a linear heat flux, yielding

$$\bar{\theta}^*_{Toki} = \int_0^{\bar{\theta}^+} \sqrt{\frac{\bar{\rho}(y)}{\bar{\rho}_w}}\frac{\tilde{c}_p(y)}{\overline{c_p}_w}\,\mathrm{d}\bar{\theta}^+. \tag{1.12}$$

Although (1.12) shows a slight improvement over (1.10), significant deviations still persist, especially near the heated wall where large property variations occur (Guo *et al.* 2022). Guo *et al.* (2018) introduced the TL scaling for thermal transformation by considering a range of thermophysical property variations

$$\bar{\theta}^+_{TL} = \int_0^{\bar{\theta}^+} \left(\frac{\overline{\rho(y)c_p^2(y)}}{\bar{\rho}_w\overline{c_p}^2_w}\right)^{1/2}\left(1+\frac{1}{2}\frac{y}{\overline{\rho(y)c_p^2(y)}}\frac{\mathrm{d}\overline{\rho(y)c_p^2(y)}}{\mathrm{d}y} - \frac{y}{\bar{\mu}(y)}\frac{\mathrm{d}\bar{\mu}(y)}{\mathrm{d}y}\right)\mathrm{d}\bar{\theta}^+. \tag{1.13}$$

Despite the modification on property variations, the improvement on T-law was shown to be limited against the VD-based transformation (Guo *et al.* 2018). This is likely due to large gradients in c_p, which cause large variations and inaccuracies in the associated terms of the TL-like derivation (Guo *et al.* 2018). Furthermore, we observe that the TL transformation in (1.13) did not account for the variations in local thermal conductivity, which could be significant in the vicinity of the pseudo-critical region. More recently, Guo *et al.* (2022) proposed an improved T-law that incorporates the contribution of viscous dissipation to the total heat flux, leading to a reduced uncertainty – by approximately 18 % – in the slope of the transformed mean temperature profiles within the logarithmic region. In spite of numerous efforts on T-law, the transformed scalar profiles still fail to collapse effectively at variable semi-local Prandtl numbers at SCP.

The primary objective of this study is to establish a theoretical framework to characterise the T-law for wall-bounded channel flows at SCP. Unlike existing approaches using temperature transformation, we introduce a novel enthalpy transformation that considers the effects of property variations sufficiently. The use of enthalpy can effectively circumvent the involvement of the isobaric specific heat gradient term, which approaches infinity across the pseudo-critical temperature, thereby remedying the large uncertainty encountered in temperature transformation. For demonstration, DNSs of fully developed SCP channel flows at different wall-temperature differences and bulk Reynolds numbers are performed for detailed examination. The remainder of this paper is structured as follows: the mathematical foundation of the enthalpy transformation is presented in § 2; the computational set-up is briefed in § 3; the performance of the new scaling law is assessed and compared with those of existing H–V relations and temperature-based scaling laws in § 4; conclusions are provided in § 5.

2. Enthalpy transformation

In light of the unsatisfactory results of the existing thermal scaling laws for SCP wall-bounded flows, we aim to develop an improved transformation for the near-wall mean scalar profiles, which can: (i) adequately account for the relevant thermophysical property

https://doi.org/10.1017/jfm.2025.11023 Published online by Cambridge University Press

variations associated with the scalar profiles, (ii) avoid the gradient of isobaric specific heat capacity-related terms, which could downgrade the overlapping performance in the transformed thermal profiles, (iii) satisfy energy balance and (iv) closely resemble the profile of wall-bounded constant-property fluid flows. To this end, we begin with the conservation equation of energy transport.

For low-speed internal flows with significant property variations due to heat transfer – such as the SCP flows considered in the present study – the low-Mach-number assumption is usually employed (Bae, Yoo & Choi 2005; Patel *et al.* 2017; Wan *et al.* 2020). Property variations due to acoustic effects and pressure changes are negligible, and heat transfer process is treated as a thermodynamically constant-pressure process. Furthermore, the viscous dissipation and gravitational work terms in the energy equation are neglected owing to their small effects in low-speed flows (Bae *et al.* 2005). With these assumptions, the energy equation is simplified as

$$\frac{\partial \rho h}{\partial t} + \frac{\partial (\rho u_j h)}{\partial x_j} = \frac{\partial}{\partial x_j}\left(\lambda \frac{\partial T}{\partial x_j}\right). \tag{2.1}$$

Introducing $\mathrm{d}h = c_p\,\mathrm{d}T$, (2.1) can be rewritten solely as a function of enthalpy

$$\frac{\partial \rho h}{\partial t} + \frac{\partial (\rho u_j h)}{\partial x_j} = \frac{\partial}{\partial x_j}\left(\alpha \frac{\partial h}{\partial x_j}\right). \tag{2.2}$$

Here, $\alpha = \lambda/c_p$, which integrates the effects of isobaric specific heat capacity and thermal conductivity. Additionally, this formulation aligns more closely with the energy conservation, compared with the traditional approach of rewriting the convection term using temperature (Patel *et al.* 2017; Chen *et al.* 2022). Equation (2.2) motivates us to derive a new scaling law based on enthalpy.

We intend to develop a universal thermal scaling law using enthalpy transformation, which enables the similarity of the mean enthalpy profiles at SCP with those of constant-property conditions in wall-bounded flows. Instead of adjusting density or isobaric specific heat capacity as seen in temperature transformation (Guo *et al.* 2018; Toki *et al.* 2020), a universal enthalpy scaling law is developed using the chain rule

$$\frac{\mathrm{d}\overline{H}}{\mathrm{d}Y} = \frac{\mathrm{d}\overline{H}}{\mathrm{d}\overline{h}} \cdot \frac{\mathrm{d}\overline{h}}{\mathrm{d}y} \cdot \frac{\mathrm{d}y}{\mathrm{d}Y}, \tag{2.3}$$

where $\overline{H}$ and Y denote the transformed universal mean enthalpy and universal wall-normal coordinate, respectively. Since $\mathrm{d}\overline{H}/\mathrm{d}\overline{h}$ and $\mathrm{d}y/\mathrm{d}Y$ are unknown, we would seek their solutions using the semi-local scaling framework (Huang *et al.* 1995) and the heat flux balance raised from the idea of stress balance condition in velocity transformation (Trettel & Larsson 2016).

The heat flux balance condition is derived from the mean energy equation. Applying Reynolds averaging to (2.2), we obtain

$$\frac{\partial \overline{\rho h}}{\partial t} + \frac{\partial \overline{\rho u_j h}}{\partial x_j} = \frac{\partial}{\partial x_j}\left(\overline{\alpha \frac{\partial h}{\partial x_j}}\right). \tag{2.4}$$

As the flow is fully developed and periodic in the x and z directions, (2.4) can be further simplified to

$$\frac{\mathrm{d}\overline{\rho v h}}{\mathrm{d}y} = \frac{\mathrm{d}}{\mathrm{d}y}\left(\overline{\alpha \frac{\mathrm{d}h}{\mathrm{d}y}}\right). \tag{2.5}$$

https://doi.org/10.1017/jfm.2025.11023 Published online by Cambridge University Press

Integrating (2.5) in the y direction yields the total heat flux equation

$$-\overline{\rho}\widetilde{v''h''}+\overline{\alpha\frac{\mathrm{d}h}{\mathrm{d}y}}=\overline{q}^{tot}, \tag{2.6}$$

where $\overline{q}^{tot}$ represents the total heat flux, that is, the sum of molecular and turbulent heat fluxes. The total heat flux should remain the same before and after transformation, leading to

$$-\overline{\rho}\widetilde{v''h''}+\overline{\alpha\frac{\mathrm{d}h}{\mathrm{d}y}}=-\overline{\rho}_w\widetilde{V''H''}+\overline{\alpha_w\frac{\mathrm{d}H}{\mathrm{d}Y}}. \tag{2.7}$$

Following Trettel & Larsson (2016), we assume that turbulent heat flux is analogous to the turbulent shear stress in the momentum equation, remaining comparable before and after transformation, and this simplifies the total heat flux balance to a balance of molecular heat flux

$$\overline{\alpha\frac{\mathrm{d}h}{\mathrm{d}y}}=\overline{\alpha_w\frac{\mathrm{d}H}{\mathrm{d}Y}}. \tag{2.8}$$

Assuming that the fluctuating molecular heat flux $\overline{\alpha'\,\partial h'/\partial y}$ embedded in (2.8) is negligible, yielding

$$\overline{\alpha}\,\frac{\mathrm{d}\overline{h}}{\mathrm{d}y}=\overline{\alpha}_w\,\frac{\mathrm{d}\overline{H}}{\mathrm{d}Y}. \tag{2.9}$$

The validity of assumptions to derive (2.8) and (2.9) will be assessed later in § 4.3. Re-arranging (2.9), we obtain

$$\frac{\mathrm{d}\overline{H}}{\mathrm{d}\overline{h}}=\frac{\overline{\alpha}}{\overline{\alpha}_w}\frac{\mathrm{d}Y}{\mathrm{d}y}. \tag{2.10}$$

Equation (2.10) provides the relationship between two transformation derivatives on the right-hand side of (2.3). We then employ the semi-local scaling framework to determine the transformation kernel $\mathrm{d}Y/\mathrm{d}y$, The scalar profile normalised by the semi-local viscous length scale (δ_v^*) is expected to be equivalent with the universal scalar profile normalised by viscous wall length scale (δ_v^+), represented as

$$\frac{Y}{\delta_v^+}=\frac{y}{\delta_v^*}. \tag{2.11}$$

Substitute the definitions of δ_v^* and δ_v^+ into (2.11), the explicit expression between Y and y is given as

$$Y=\frac{\overline{\mu}_w}{\overline{\mu}(y)}\sqrt{\frac{\overline{\rho}(y)}{\overline{\rho}_w}}\,y, \tag{2.12}$$

where dynamic viscosity and density vary with the wall-normal coordinate y. The derivative of the universal wall-normal coordinate Y with respect to y can be derived as follows:

$$\frac{\mathrm{d}Y}{\mathrm{d}y}=\frac{\overline{\mu}_w}{\overline{\mu}(y)}\sqrt{\frac{\overline{\rho}(y)}{\overline{\rho}_w}}\left[1-\frac{y}{\overline{\mu}(y)}\frac{\mathrm{d}\overline{\mu}(y)}{\mathrm{d}y}+\frac{y}{2\overline{\rho}(y)}\frac{\mathrm{d}\overline{\rho}(y)}{\mathrm{d}y}\right]. \tag{2.13}$$

https://doi.org/10.1017/jfm.2025.11023 Published online by Cambridge University Press

Cases	$\Delta T^{\dagger}$(K)	$T^{\dagger}_{wc}$(K)	$T^{\dagger}_{wh}$(K)	$\rho^{\dagger}_{wc}/\rho^{\dagger}_{wh}$	Re
Const-5705	20	297.8	317.8	1.00	5705
T20-5705	20	297.8	317.8	3.21	5705
T100-5705	100	257.8	357.8	6.68	5705
T150-5705	150	232.8	382.8	8.46	5705
T100-13981	100	257.8	357.8	6.68	13 981

Table 1. Key parameters of different cases: $\Delta T^{\dagger}$ (temperature difference), $T^{\dagger}_{wc}$ (cooled-wall temperature), $T^{\dagger}_{wh}$ (heated-wall temperature), $\rho^{\dagger}_{wc}/\rho^{\dagger}_{wh}$ (density ratio).

Substituting (2.13) into (2.10) yields

$$\frac{\mathrm{d}\overline{H}}{\mathrm{d}\overline{h}} = \frac{\overline{\alpha}(y)}{\overline{\alpha}_w} \cdot \frac{\overline{\mu}_w}{\overline{\mu}(y)} \sqrt{\frac{\overline{\rho}(y)}{\overline{\rho}_w}} \left[1 - \frac{y}{\overline{\mu}(y)} \frac{\mathrm{d}\overline{\mu}(y)}{\mathrm{d}y} + \frac{y}{2\overline{\rho}(y)} \frac{\mathrm{d}\overline{\rho}(y)}{\mathrm{d}y} \right]. \tag{2.14}$$

Through dimensional analysis, we define the friction enthalpy as $\bar{h}_\tau = \overline{q}_w/(\overline{\rho}_w \bar{u}_\tau)$. Dividing both numerator and denominator by friction enthalpy on the left-hand side of (2.14), the transformed scalar profile based on enthalpy is deduced by integration

$$\overline{H}^{+} = \int_0^{\overline{h}^{+}} \frac{\overline{\alpha}(y)}{\overline{\alpha}_w} \cdot \frac{\overline{\mu}_w}{\overline{\mu}(y)} \sqrt{\frac{\overline{\rho}(y)}{\overline{\rho}_w}} \left[1 - \frac{y}{\overline{\mu}(y)} \frac{\mathrm{d}\overline{\mu}(y)}{\mathrm{d}y} + \frac{y}{2\overline{\rho}(y)} \frac{\mathrm{d}\overline{\rho}(y)}{\mathrm{d}y} \right] \mathrm{d}\overline{h}^{+}, \tag{2.15}$$

where the superscript '+' denotes the variables normalised by friction enthalpy. Here, $\overline{H}^{+}$, defined in (2.15), is the new thermal scaling law using enthalpy transformation. Unlike conventional temperature-based transformations, enthalpy transformation incorporates property variations, including mean density, viscosity and thermal diffusivity. Meanwhile, it excludes the gradient of isobaric specific heat-related derivative terms that could amplify errors in thermal scaling.

Alternatively, the scaling law can also be written as a function of the semi-local wall-normal coordinate

$$\overline{H}^{+} = \int_0^{y^*} \frac{\partial \overline{H}^{+}}{\partial y^*} \mathrm{d}y^* = \int_0^{y^*} \overline{\alpha}^{+} \frac{\partial \overline{h}^{+}}{\partial y^{+}} \mathrm{d}y^*, \tag{2.16}$$

where $\overline{\alpha}^{+} = \overline{\alpha}(y)/\overline{\alpha}_w$. In the following, the proposed enthalpy scaling law is examined using DNS data of SCP channel flows with various wall-temperature differences and Reynolds numbers. For comparison, existing temperature-based thermal scaling laws are also discussed.

3. Computational set-up

Table 1 summarises the key parameters of all the DNS cases in SCP channel flows. In all cases, the working fluid is CO_2, and the operating pressure $P_0^{\dagger}$ is maintained at a value of 8 MPa, corresponding to a reduced pressure $p_r = 1.1$. The thermophysical properties of CO_2 at this pressure are depicted in figure 1. Both the upper and lower walls of the channel serve as isothermal boundaries, and $T^{\dagger}_{wc}$ and $T^{\dagger}_{wh}$ denote the temperature of cooled and heated channel walls. The const-5705 case represents a constant-property flow, while the remaining four cases operate at SCP, where the temperature differences range from 20 to 150 K to examine various heating conditions. The setting of temperature span in each SCP case ensures the occurrence of the pseudo-critical process. The bulk Reynolds

https://doi.org/10.1017/jfm.2025.11023 Published online by Cambridge University Press

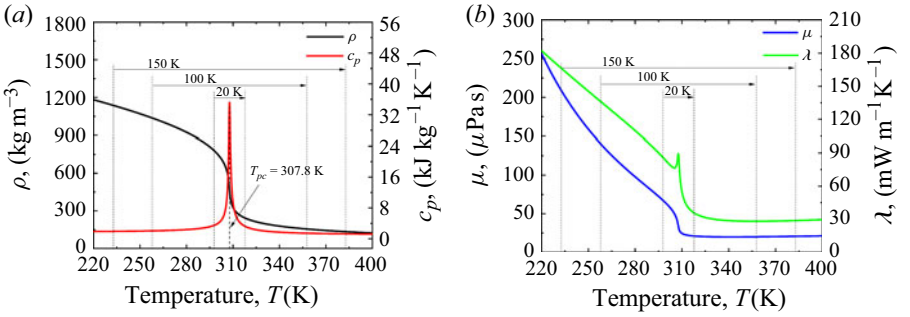


Figure 1. Thermophysical properties of CO_2 at 8.0 MPa: (*a*) density ρ and isobaric specific heat c_p, and (*b*) thermal conductivity λ and dynamic viscosity μ as functions of temperature.

numbers for cases T20-5705, T100-5705 and T150-5705 are set at a constant value of $Re = 5705$, while case T100-13981 has a bulk Reynolds number of $Re = 13\,981$. All Reynolds numbers are calculated based on the bulk velocity and the channel height, using the characteristic thermophysical properties at the pseudo-critical temperature. Note that the const-5705 case serves as a reference for all other cases, as our goal is to develop a transformation that aligns the transformed scalar profiles of SCP fluid flows with that of constant-property flow.

The numerical scheme implements a kinetic-energy-conservative space–time discretisation (Pierce & Moin 2004), with fourth-order central differencing for spatial derivatives and a semi-implicit iterative algorithm (Wall, Pierce & Moin 2002). To mitigate numerical oscillations caused by steep enthalpy gradients, a fifth-order weighted essentially non-oscillatory scheme is applied. Thermophysical properties, including density, are interpolated from pre-tabulated data as functions of enthalpy and constant thermodynamic pressure (8 MPa), generated using the NIST REFPROP database (Lemmon *et al.* 2018). Details of the computational set-up, grid resolution and code verification can be found in the previous studies (Wan *et al.* 2020, 2025).

4. Assessment of enthalpy transformation

Before assessing the performance of thermal transformations, we first examine the behaviour of the mean isobaric specific heat capacity and thermal conductivity, along with their fluctuations at SCP. Unlike in atmospheric flows, these properties show abrupt variations with temperature in SCP fluid flows. As shown in figure 2(*a*), $\bar{c}_p$ exhibits pronounced variation on the heated-wall side ($y = 2.0$), which becomes increasingly significant with higher wall-temperature difference (higher density ratio). In particular, for the T150-5705 case, figure 2(*c*) reveals that the root mean square (r.m.s.) of isobaric specific capacity fluctuations of c_p can reach up to 150 % of the mean value (the r.m.s. of fluctuation is defined as $\phi'_{rms} = \sqrt{\overline{\phi^2} - \bar{\phi}^2}$). This highlights the substantial impact of c_p variation on the thermal boundary-layer structure, an effect often neglected in conventional scaling approaches. To further substantiate this point, we have also included the wall-normal distributions of mean thermal conductivity ($\bar{\lambda}$) and its relative fluctuations in figures 2(*b*) and 2(*d*), respectively. The results show that the r.m.s. of thermal conductivity fluctuations can reach up to 45 % of its mean value. These property variations are not properly considered by temperature-based scaling methods, thereby limiting their predictive performance.

https://doi.org/10.1017/jfm.2025.11023 Published online by Cambridge University Press

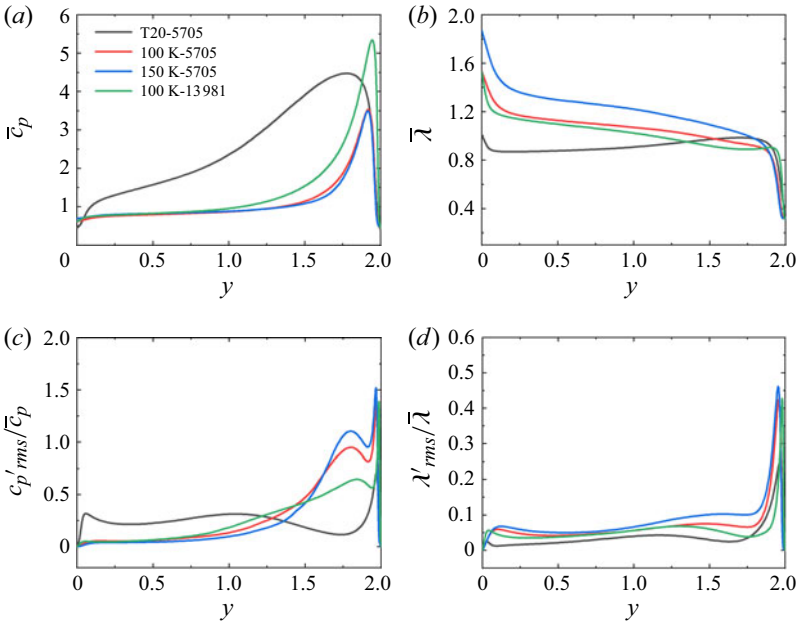


Figure 2. Wall-normal mean profiles of (*a*) isobaric specific heat capacity $\bar{c}_p$, and (*b*) thermal conductivity $\bar{\lambda}$; and r.m.s. profiles of (*c*) $c_p{}'_{rms}/\bar{c}_p$, and (*d*) $\lambda'_{rms}/\bar{\lambda}$, normalised by local mean quantities.

4.1. *Comparison with H–V relations*

The performance of the new transformation is first assessed against existing H–V relations. Specifically, we compared the mean enthalpy profiles predicted by the H–V relations of Duan & Martin (2011) and Li *et al.* (2025) and by our proposed enthalpy transformation with those obtained from DNSs. Figure 3 presents the wall-normal profiles of the enthalpy $\tilde{h}$ obtained from each H–V relation and the proposed transformation, as well as the DNS data. On the cooled-wall side, where the fluid thermodynamic state remains far from the pseudo-boiling region, both our transformation and the H–V relation of Li *et al.* (2025) show good agreement with DNS results, whereas the relation of Duan & Martin (2011) exhibits slightly poor performance (blue dashed lines). This is likely due to the empirical nature of the function $f(\tilde{u}/\tilde{u}_e)$, which was obtained by only fitting the DNS data of hypersonic reacting turbulent boundary layers. Additionally, the recovery factor is typically treated as a constant (determined by a constant Pr), which is not applicable to SCP flows where Pr varies significantly. The accuracy may be improved by fitting the coefficients of the empirical function using the present DNS results.

On the heated-wall side, however, both H–V relations deviate substantially from DNS results, while the proposed transformation remains in close agreement. Notably, the formulation by Li *et al.* (2025) even produces unphysical values ($\tilde{h} > 1$) in the region $y^* < 10$. This deficiency likely arises from the strong transcritical effects and sharp thermophysical gradients near the heated wall, which are not carefully considered by the generalised recovery factor r_g^*, as it accounts only for wall properties.

To further quantify these differences, we introduce the integrated relative error (Chen *et al.* 2025; Zhu *et al.* 2025), defined as

$$\epsilon_{y^*}(\%) = \frac{\int_0^{y^*} |\Theta - \Theta_{ref}|\,\mathrm{d}y^*}{\int_0^{y^*} \Theta_{ref}\,\mathrm{d}y^*} \times 100\,\%, \tag{4.1}$$

https://doi.org/10.1017/jfm.2025.11023 Published online by Cambridge University Press

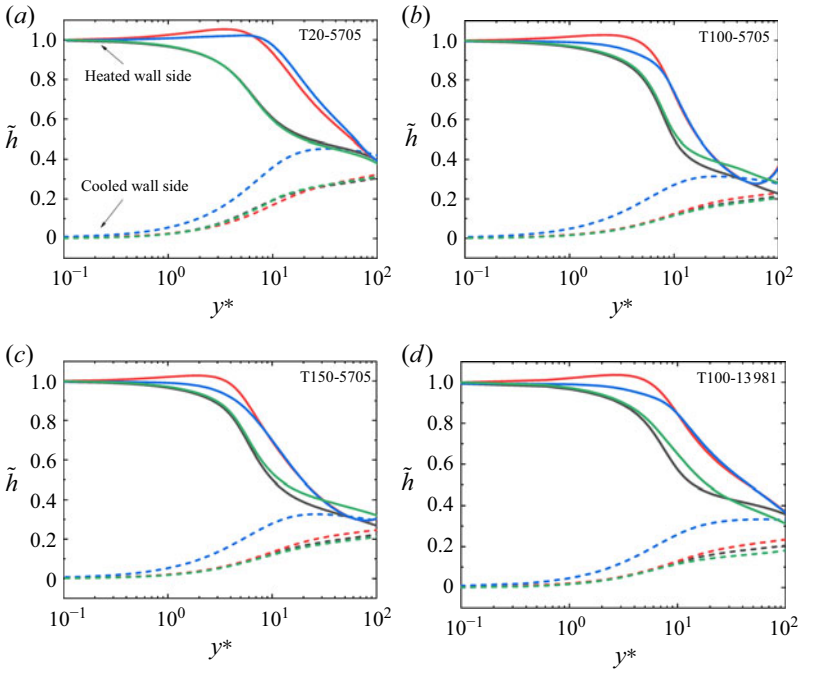


Figure 3. Comparison of mean enthalpy profiles obtained from different methods with DNS results in various cases: (*a*) T20-5705, (*b*) T100-5705, (*c*) T150-5705 and (*d*) T100-13981. Black: DNS results; red: H–V relation (Li *et al.* 2025); blue: H–V relation (Duan & Martin 2011); green: present enthalpy transformation.

where Θ and Θ_{ref} represent the predicted and reference quantities, respectively, with DNS data serving as the reference. Figure 4 presents the distributions of the integrated relative error along y^* for each SCP case on both the cooled- and heated-wall sides.

Consistent with the observations above, the proposed transformation shows comparable accuracy to the H–V relation by Li *et al.* (2025) on the cooled-wall side. On the heated-wall side, however, both H–V relations display notable deviations, while the proposed transformation yields relatively small errors, demonstrating its robustness and reliability under SCP conditions. These results also suggest that existing H–V relations, originally developed for high-speed compressible flows under the perfect-gas assumption, cannot be directly extended to SCP flows where real-fluid effects dominate.

4.2. *Comparison with temperature-based transformations*

Next, we evaluate the comparable performance of the proposed transformation against several previously established temperature-based scaling methods. Figure 5 shows the transformed scalar profiles of all cases using different scaling laws, including existing temperature transformations $\overline{\theta}^*$ (1.10), $\overline{\theta}^*_{Toki}$ (1.12), $\overline{\theta}^+_{VD}$ (Guo *et al.* 2018), $\overline{\theta}^+_{TL}$ (1.13) and the proposed enthalpy transformation $\overline{H}^+$ (2.15). For consistency, all profiles are normalised by Pr_w to eliminate the influence of the wall Prandtl number, and all vertical axes have been set to the same range of the scale. As shown in figure 5(*a–d*), the transformed scalar profiles based on temperature transformation overlap unsatisfactorily near the cooled wall and fail largely near the heated wall. This is consistent with the findings of existing studies (Guo *et al.* 2018, 2022). This discrepancy likely stems from inadequate consideration of variations in thermophysical properties, including

https://doi.org/10.1017/jfm.2025.11023 Published online by Cambridge University Press

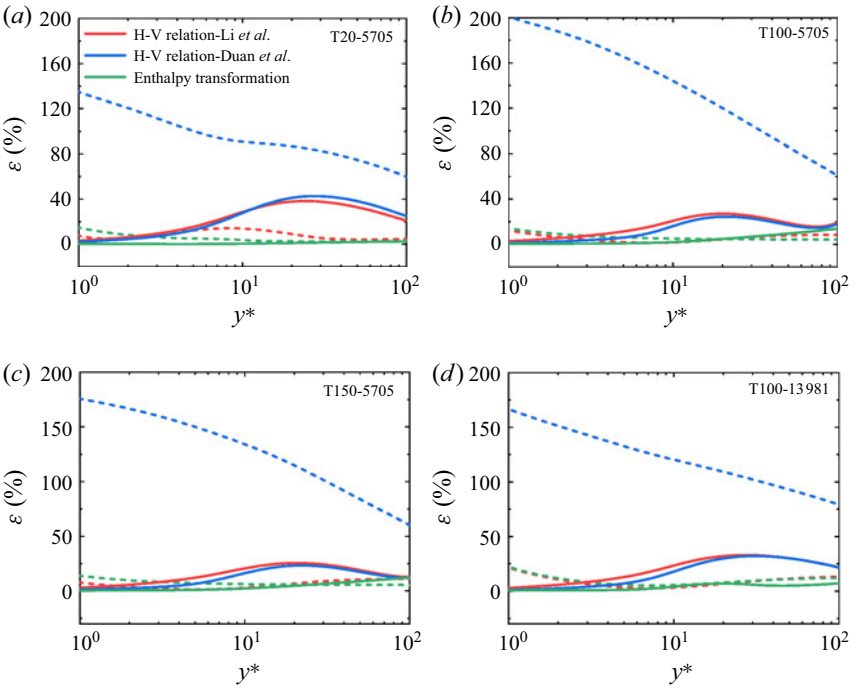


Figure 4. Integrated relative errors of different methods in cases (*a*) T20-5705, (*b*) T100-5705, (*c*) T150-5705 and (*d*) T100-13981. Solid lines: heated-wall side; dashed lines: cooled-wall side.

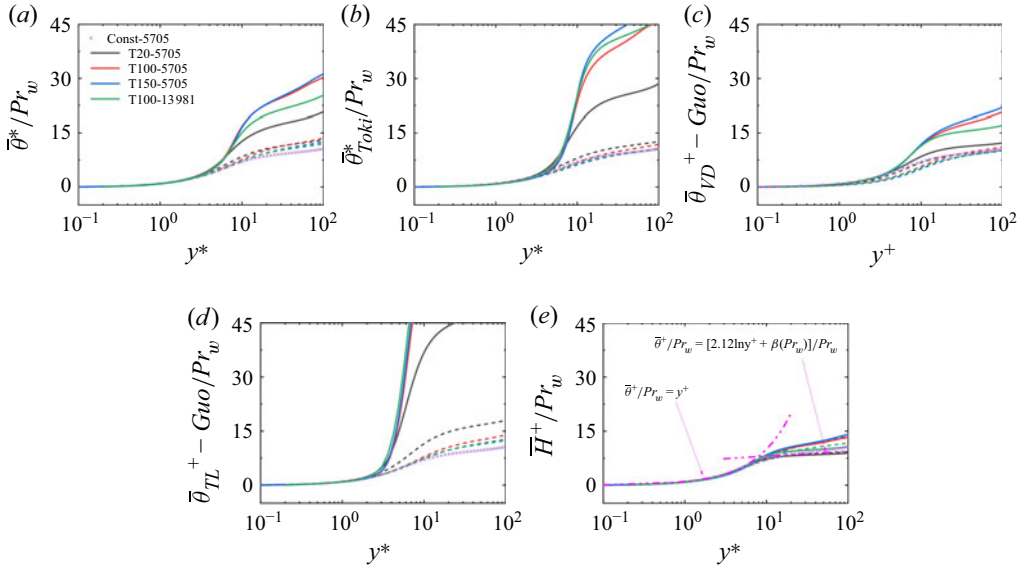


Figure 5. Transformed scalar profiles of (*a*) $\overline{\theta}^*/Pr_w$, (*b*) $\overline{\theta}^*_{Toki}/Pr_w$, (*c*) $\overline{\theta}^+_{VD} - Guo/Pr_w$, (*d*) $\overline{\theta}^+_{TL} - Guo/Pr_w$ and (*e*) $\overline{H}^+/Pr_w$. Solid lines: cooled-wall side; dashed lines: heated-wall side; magenta dash-dot line: Kader's law.

https://doi.org/10.1017/jfm.2025.11023 Published online by Cambridge University Press

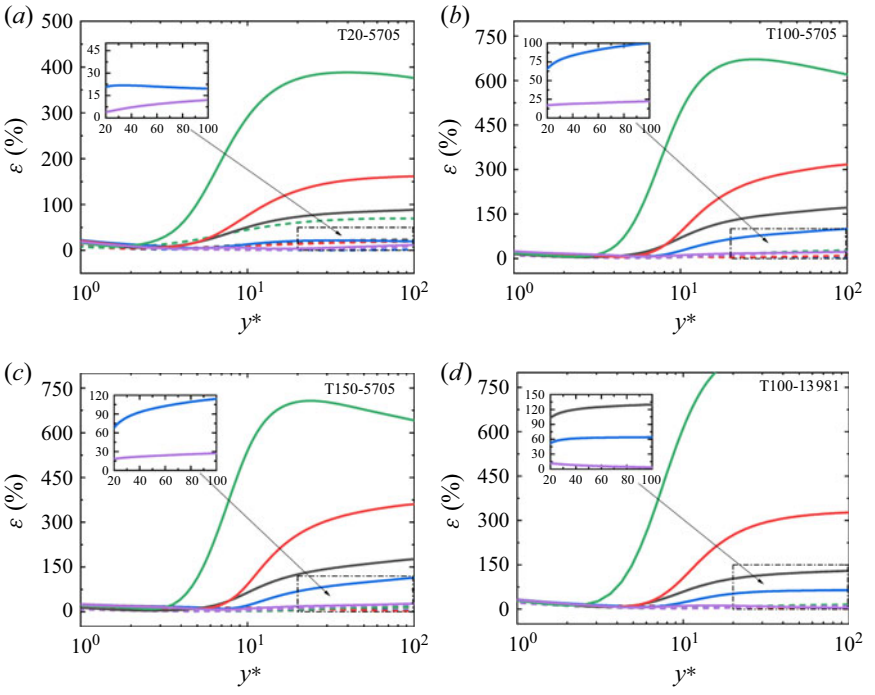


Figure 6. Integrated relative errors of mean thermal scaling laws in different cases: (*a*) T20-5705, (*b*) T100-5705, (*c*) T150-5705 and (*d*) T100-13981. Solid lines: heated-wall side; dashed lines: cooled-wall side. Black lines: $\bar{\theta}^*$; red lines: $\bar{\theta}^*_{Toki}$; blue lines: $\bar{\theta}^+_{VD} - Guo$; green lines: $\bar{\theta}^+_{TL} - Guo$; and purple lines: $\bar{H}^+$. Note that the error profiles in the logarithmic region on the heated-wall side are zoomed in for clarity.

thermal conductivity and dynamic viscosity, on the heated-wall side, where the pseudo-critical phenomenon occurs (Wan *et al.* 2025). Under this condition, strong fluctuations and substantial mean variations of thermophysical properties, particularly specific heat capacity, are triggered, leading to the failure of the temperature-based scaling law. In contrast, the newly proposed enthalpy transformation (figure 5*e*) exhibits good overlapping performance in the viscous sublayer and the buffer layer near both cooled and heated walls. Notably, in the logarithmic region, the alignment of the new transformed scalar curves is substantially improved, compared with the temperature-based scalar curves.

To further quantify the alignment performance, figure 6 shows the distributions of the integrated relative error along the wall-normal distance y^* in each case on both the cooled- and heated-wall sides. On the cooled-wall side, where the thermodynamic state is far from the pseudo-boiling point and property variations are gradual, all transformation methods yield relatively small errors, and the proposed enthalpy-based transformation performs similarly to previously developed temperature-based transformations. On the heated-wall side, in contrast, the enthalpy-based transformation exhibits markedly smaller errors than the existing temperature-based methods. To evaluate the performance in the logarithmic region, the relative root-mean-square error (rRMSE) of the transformed profiles is computed as

$$\mathrm{RMSE} = \sqrt{\frac{1}{N}\sum_{i=1}^{N}(\Theta_i - \Theta_{ref,i})^2}, \quad \mathrm{r.m.s.} = \sqrt{\frac{1}{N}\sum_{i=1}^{N}\Theta_{ref,i}^2}, \tag{4.2}$$

https://doi.org/10.1017/jfm.2025.11023 Published online by Cambridge University Press

Cases	$\bar{\theta}^*$	$\bar{\theta}^*_{Toki}$	$\bar{\theta}^+_{VD}$	$\bar{\theta}^*_{TL}$	$\bar{H}^+$
T20-5705	65.9 %	118.2 %	15.4 %	284.1 %	9.9 %
T100-5705	131.7 %	243.0 %	76.0 %	496.6 %	21.7 %
T150-5705	139.0 %	285.3 %	89.6 %	526.4 %	25.9 %
T100-13981	96.5 %	244.2 %	48.4 %	639.3 %	8.4 %

Table 2. The rRMSE of different transformed profiles against constant-property case.

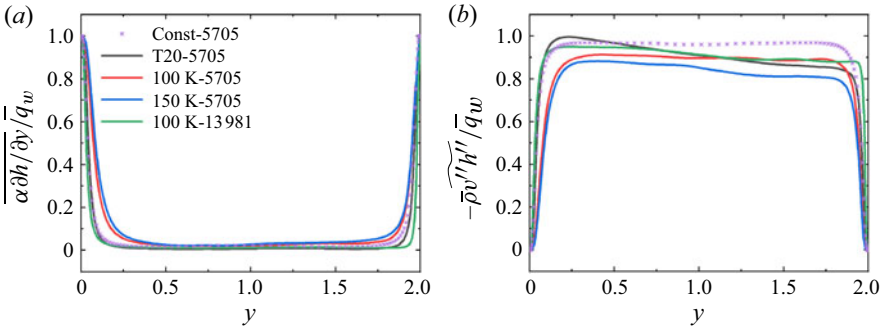


Figure 7. Decomposition of the total heat flux into (*a*) the molecular heat flux $\overline{\alpha\ \partial h/\partial y}$ and (*b*) the turbulent heat flux $-\bar{\rho}\ \widetilde{v''h''}$. All cases are normalised by the wall molecular heat flux $\bar{q}_w$.

$$\text{rRMSE} = \frac{\text{RMSE}}{\text{RMS}} \times 100\,\%. \tag{4.3}$$

Table 2 summarises the rRMSE values for each SCP case relative to the constant-property baseline, specifically within $30 < y^* < 100$. The results confirm that the proposed transformation consistently achieves the lowest rRMSE values across both small and large wall-temperature differences. Notably, the superiority of enthalpy-based scaling becomes more pronounced at larger wall-temperature differences.

4.3. *Uncertainty analysis*

Note that slight misalignment still persists in figure 5(*e*), which is probably linked to the earlier assumptions made to derive (2.8) and (2.9): (i) reducing the total heat flux balance to the molecular heat flux balance; and (ii) neglecting the fluctuating component of molecular heat flux. The validity of (2.8) is examined in figure 7, where the normalised mean molecular heat flux $\overline{\alpha\ \partial h/\partial y}$ and the turbulent heat flux $-\bar{\rho}\ \widetilde{v''h''}$ are compared between the SCP and constant-property cases. It is observed that $\overline{\alpha\ \partial h/\partial y}$ dominates in the vicinity of the cooled and heated walls, while $-\bar{\rho}\ \widetilde{v''h''}$ dominates away from the channel walls. The non-negligible differences in turbulent heat flux between SCP and constant-property cases exist away from the wall. These discrepancies help explain the observed deviations in the transformed enthalpy profiles in the logarithmic region, which is also an area we strive to improve in the future.

To evaluate assumption (ii), figure 8 presents the distributions of $\overline{\alpha\ \partial h/\partial y}$ and $\overline{\alpha}\ \overline{\partial h/\partial y}$, each normalised by wall heat flux. The difference between the two terms reflects the relative contribution of fluctuating molecular heat flux. The two quantities align well on the cooled-wall side. On the hot-wall side, however, notable discrepancies appear in the buffer and logarithmic regions. To quantify the effect of the fluctuating term, table 3 presents the rRMSE between the true value $\overline{\alpha\ \partial h/\partial y}$ and the simplified value $\overline{\alpha}\ \overline{\partial h/\partial y}$ using data

https://doi.org/10.1017/jfm.2025.11023 Published online by Cambridge University Press

Cases	T20-5705	T100-5705	T150-5705	T100-13981
Cooled-wall side	2.19 %	1.44 %	1.04 %	1.34 %
Heated-wall side	9.24 %	13.50 %	15.86 %	10.31 %

Table 3. Relative deviation between the truth $\overline{\alpha\ \partial h/\partial y}$ and the simplification $\overline{\alpha}\,\overline{\partial h/\partial y}$ in different cases.

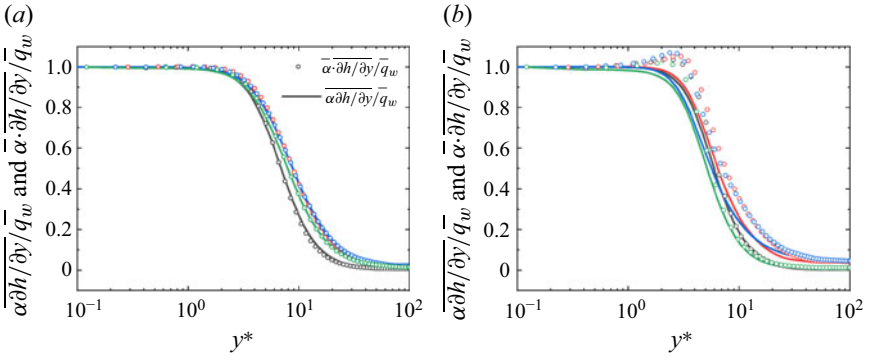


Figure 8. Effect of the fluctuating molecular heat flux: (*a*) cooled side, (*b*) heated side. Solid lines: $\overline{\alpha\partial h/\partial y}$, symbols: $\bar{\alpha}\,\overline{\partial h/\partial y}$. Black: T20-5705, red: T100-5705, blue: T150-5705, green: T100-13981.

points within the near-wall region where $y^* < 100$. The results show that rRMSE is small in all cases on the cooled-wall side, where the fluid thermodynamic states are far away from the pseudo-critical point and the variations in thermal diffusivity are small. The contribution of the fluctuating molecular heat flux is thus negligible on the cooled-wall side. In contrast, on the heated-wall side, especially under high temperature differences, the influence of neglected fluctuation becomes pronounced. For example, in the T150-5705 case, the rRMSE reaches 15.86 %, implying that the neglected fluctuation contributes to the deviation observed in the transformed profiles near the heated wall.

Despite small discrepancies, the proposed enthalpy transformation under the present assumptions shows the remarkable performance on the alignment of thermal profiles compared with the existing temperature-based transformations in the literature. For wall-bounded turbulence and heat transfer under SCP conditions, the energy equation can be more effectively unified using enthalpy as the primary variable. In engineering applications, enthalpy at the wall can be determined from wall-temperature measurements, and the enthalpy distribution in channel flows can be reconstructed using the enthalpy-based scaling law proposed in this study. The temperature profile can be subsequently retrieved through thermodynamic calculations. Note that the proposed enthalpy transformation is examined in SCP channel flows in the present work; its validity in other wall-bounded SCP flows remains to be verified and will be explored in the future.

5. Conclusion

A novel thermal scaling law based on enthalpy transformation has been developed to address the limitations of existing wall-scaling laws under SCP conditions. The proposed transformation is derived from the chain rule, heat flux balance and semi-local scaling framework, enabling a consistent treatment of thermophysical property variations while excluding the gradient of isobaric specific heat-related derivative terms. The transformed

https://doi.org/10.1017/jfm.2025.11023 Published online by Cambridge University Press

mean enthalpy profiles show good overlapping performance in the viscous sublayer and the buffer layer. In the logarithmic region, the curves also demonstrate significantly improved alignment with those of constant-property incompressible flows, although some deviations persist under high density ratio conditions. Compared with existing H–V relations, the new scaling also provides better performance, particularly near the heated wall where the pseudo-boiling process occurs with abrupt thermophysical property variations. Overall, the proposed enthalpy-based scaling provides a robust and physically consistent approach for characterising near-wall scalar behaviours in SCP channel flows, offering new insights for modelling and analysis in real-fluid environments.

Fundings. This work is supported by the National Natural Science Foundation of China (52276123), the China Postdoctoral Science Foundation (2024M751636) and the Postdoctoral Fellowship Program of CPSF (GZC20231221).

Declaration of interests. The authors report no conflict of interest.

Data availability statement. Data availability statement. The data that support the findings of this study are available from the corresponding author upon reasonable request.

References

BAE, J.H., YOO, J.Y. & CHOI, H. 2005 Direct numerical simulation of turbulent supercritical flows with heat transfer. *Phys. Fluids* **17** (10), 105104.

BAI, T., GRIFFIN, K.P. & FU, L. 2022 Compressible velocity transformations for various noncanonical wall-bounded turbulent flows. *AIAA J.* **60** (7), 4325–4337.

BRADSHAW, P. & HUANG, G.P. 1995 The law of the wall in turbulent flow. *Proc. R. Soc. Lond. A* **451** (1941), 165–188.

BUSEMANN, A. 1931 *Handbuch der Experimentalphysik*, vol. 4. Geest und Portig.

BUSCHMANN, M.H. & GAD-EL-HAK, M. 2006 Recent developments in scaling of wall-bounded flows. *Prog. Aerosp. Sci.* **42** (5–6), 419–467.

CHEN, P.E., HUANG, G.P., SHI, Y., YANG, X.I. & LV, Y. 2022 A unified temperature transformation for high-Mach-number flows above adiabatic and isothermal walls. *J. Fluid Mech.* **951**, A38.

CHEN, X., GAN, J. & FU, L. 2025 Mean temperature–velocity relation and a new temperature wall model for compressible laminar and turbulent flows. *J. Fluid Mech.* **1009**, A39.

CHENG, C. & FU, L. 2024 Mean temperature scalings in compressible wall turbulence. *Phys. Rev. Fluids* **9**, 054610.

DUAN, L. & MARTIN, M. 2011 Direct numerical simulation of hypersonic turbulent boundary layers. Part 4. Effect of high enthalpy. *J. Fluid Mech.* **684**, 25–59.

GRIFFIN, K.P., FU, L. & MOIN, P. 2021 Velocity transformation for compressible wall-bounded turbulent flows with and without heat transfer. *Proc. Natl Acad. Sci. USA* **118** (34), e2111144118.

GUO, J., YANG, X.I.A. & IHME, M. 2018 Thermal structures and heat transfer in wall-bounded flows at transcritical conditions. *CTR Annu. Res. Briefs* 273–284.

GUO, J., YANG, X.I.A. & IHME, M. 2022 Structure of the thermal boundary layer in turbulent channel flows at transcritical conditions. *J. Fluid Mech.* **934**, A45.

HASAN, A.M., LARSSON, J., PIROZZOLI, S. & PECNIK, R. 2023 Incorporating intrinsic compressibility effects in velocity transformations for wall-bounded turbulent flows. *Phys. Rev. Fluids* **8** (11), L112601.

HUANG, P.G., COLEMAN, G.N. & BRADSHAW, P. 1995 Compressible turbulent channel flows: DNS results and modelling. *J. Fluid Mech.* **305**, 185–218.

HUANG, P.G., COLEMAN, G.N., SPALART, P.R. & YANG, X.I.A. 2023 Velocity and temperature scalings leading to compressible laws of the wall. *J. Fluid Mech.* **977**, A49.

JIANG, P.-X., ZHANG, Y., XU, Y.-J. & SHI, R.-F. 2008 Experimental and numerical investigation of convection heat transfer of CO_2 at supercritical pressures in a vertical tube at low Reynolds numbers. *Intl J. Therm. Sci.* **47**, 998–1011.

KADER, B.A. 1981 Temperature and concentration profiles in fully turbulent boundary layers. *Intl J. Heat Mass Transfer* **24** (9), 1541–1544.

LEE, J., JUNG, S.Y., SUNG, H.J. & ZAKI, T.A. 2014 Turbulent thermal boundary layers with temperature-dependent viscosity. *Intl J. Heat Fluid Flow* **49**, 43–52.

https://doi.org/10.1017/jfm.2025.11023 Published online by Cambridge University Press

LEMMON, E.W., BELL, I.H., HUBER, M.L. & MCLINDEN, M.O. 2018 *NIST Standard Reference Database 23: Reference Fluid Thermodynamic and Transport Properties (REFPROP), Version 10.0*. National Institute of Standards and Technology. Standard Reference Data Program.

LI, B., ZHANG, Y.-S., DUAN, L. & CHOUDHARI, M.M. 2025 Improved wall function method for hypersonic reacting turbulent boundary layers. *AIAA J.* **63** (1), 55–71.

MA, P.C., YANG, X.I.A. & IHME, M. 2018 Structure of wall-bounded flows at transcritical conditions. *Phys. Rev. Fluids* **3** (3), 034609.

MO, F., ZHANG, Y.-S., DUAN, L. & CHOUDHARI, M.M. 2023 Direct numerical simulation of hypersonic wall-bounded turbulent flows: an improved inflow boundary condition and applications. *Phys. Fluids* **35** (3), 035135.

PATEL, A., BOERSMA, B.J. & PECNIK, R. 2017 Scalar statistics in variable property turbulent channel flows. *Phys. Rev. Fluids* **2** (8), 084604.

PECNIK, R. & PATEL, A. 2017 Scaling and modelling of turbulence in variable property channel flows. *J. Fluid Mech.* **823**, R1.

PIERCE, C.D. & MOIN, P. 2004 Progress-variable approach for large-eddy simulation of non-premixed turbulent combustion. *J. Fluid Mech.* **504**, 73–97.

POPE, S.B. 2001 Turbulent flows. *Meas. Sci. Technol.* **12** (11), 2020.

PRANDTL, L. 1925 Bericht über Untersuchungen zur ausgebildeten Turbulenz. *ZAMM* **5** (2), 136–139.

REN, J., WU, Y.X., MAO, X.R., WANG, C. & KLOKER, M. 2025 Sensitivity of three-dimensional boundary layer stability to intrinsic uncertainties of fluid properties: a study on supercritical CO_2. *J. Fluid Mech.* **1007**, A7.

TOKI, T., TERAMOTO, S. & OKAMOTO, K. 2020 Velocity and temperature profiles in turbulent channel flow at supercritical pressure. *J. Propul. Power* **36** (1), 3–13.

TRETTEL, A. & LARSSON, J. 2016 Mean velocity scaling for compressible wall turbulence with heat transfer. *Phys. Fluids* **28** (2), 026102.

VAN DRIEST, E.R. 1951 Turbulent boundary layer in compressible fluids. *J. Aeronaut. Sci.* **18** (3), 145–160.

VON KARMAN, T. 1939 The analogy between fluid friction and heat transfer. *Trans. ASME* **61** (8), 705–710.

WALL, C., PIERCE, C.D. & MOIN, P. 2002 A semi-implicit method for resolution of acoustic waves in low mach number flows. *J. Comput. Phys.* **181** (2), 545–563.

WALZ, A. 1969 *Boundary Layers of Flow and Temperature*. MIT Press.

WAN, T., WANG, X.J., JIN, Y.X. & ZHAO, P.H. 2025 Effects of large density variations on near-wall turbulence and heat transfer in channel flow at supercritical pressure. *J. Fluid Mech.* **1007**, A68.

WAN, T., ZHAO, P., LIU, J., WANG, C. & LEI, M. 2020 Mean velocity and temperature scaling for near-wall turbulence with heat transfer at supercritical pressure. *Phys. Fluids* **32** (5), 055103.

WANG, X., HUO, H., UNNIKRISHNAN, U. & YANG, V. 2018 A systematic approach to high-fidelity modeling and efficient simulation of supercritical fluid mixing and combustion. *Combust. Flame* **195**, 203–215.

WHITE, M.T., BIANCHI, G., CHAI, L., TASSOU, S.A. & SAYMA, A.I. 2021 Review of supercritical CO_2 technologies and systems for power generation. *Appl. Therm. Engng* **185**, 116447.

XIE, G., XIAOXIAO, X., XIANLIANG, L., ZHOUHANG, L. & YONG, L. 2022 Heat transfer behaviors of some supercritical fluids: a review. *Chin. J. Aeronaut.* **35**, 290–306.

YANG, V. 2000 Modeling of supercritical vaporization, mixing, and combustion processes in liquid-fueled propulsion systems. *Proc. Combust. Inst.* **28**, 925–942.

YOO, J.Y. 2013 The turbulent flows of supercritical fluids with heat transfer. *Annu. Rev. Fluid Mech.* **45** (1), 495–525.

ZHANG, C., DUAN, L. & CHOUDHARI, M.M. 2018 Direct numerical simulation database for supersonic and hypersonic turbulent boundary layers. *AIAA J.* **56** (11), 4297–4311.

ZHANG, Y.S., BI, W.T., HUSSAIN, F., LI, X.L. & SHE, Z.S. 2012 Mach-number-invariant mean-velocity profile of compressible turbulent boundary layers. *Phys. Rev. Lett.* **109** (5), 054502.

ZHANG, Y.-S., DUAN, L., CHOUDHARI, M. & WU, M. 2014 A generalized Reynolds analogy for compressible wall-bounded turbulent flows. *J. Fluid Mech.* **739**, 392–420.

ZHU, X., SONG, Y., YANG, X. & XIA, Z. 2024 Velocity transformation for compressible wall-bounded turbulence—an approach through the mixing length hypothesis. *Sci. China Phys. Mech. Astron.* **67** (9), 294711.

ZHU, X., ZHANG, P., YANG, X., JI, Y. & XIA, Z. 2025 A unified framework for mean temperature analysis in compressible turbulent channel flows. *J. Fluid Mech.* **1012**, R2.

https://doi.org/10.1017/jfm.2025.11023 Published online by Cambridge University Press